

Catechol-Based Macrocyclic Rods: En Route to Redox-Active Molecular Switches

Nicolas Weibel,^[a] Artem Mishchenko,^[b] Thomas Wandlowski,^{*[b]} Markus Neuburger,^[a] Yann Leroux,^[a] and Marcel Mayor^{*[a,c]}

Keywords: Molecular electronics / Macrocycles / Molecular rods / Catechol / Electrochemistry / Single-molecule conductance

The design and synthesis of the macrocyclic turnstile **1** comprising a terminally sulfur-functionalized molecular rod and a redox-active catechol subunit is described. The shape-persistent macrocyclic scaffold consists of alternating arylene and ethynylene units. A freely rotating 2,6-diethynyl-catechol subunit is clamped between both terminal arylene subunits as molecular turnstile. While the electrochemical switching between the catechol and the quinone form of this catechol subunit is displayed by cyclic voltammetry, conformational rearrangements by favoring and disfavoring the formation of intramolecular hydrogen bonds are the subject of

current investigations. Terminal acetyl-protected sulfur anchor groups enabled the immobilization of the macrocycle between an Au tip and an Au substrate of a STM set-up. Preliminary single-molecule transport investigations of the turnstile **1** display comparable values as for the parent molecular rod. An electrochemically-controlled single-molecule transport experiment to investigate redox-state-dependent transport properties is currently under way.

(© Wiley-VCH Verlag GmbH & Co. KGaA, 69451 Weinheim, Germany, 2009)

Introduction

In the field of molecular electronics, tailor-made molecules are promising candidates as potential functional units in electronic circuits, owing to their minute size and rich structural variety.^[1–6] In recent years, interesting correlations between transport properties and molecular structure have been deduced from the investigation of single-molecule junctions and self-assembled monolayers (SAMs).^[7–10] In our own labs numerous features effecting single-molecule transport properties have been investigated like the structures' symmetry,^[11] the relative position of anchoring groups,^[12] the division of the π -system,^[13] the length of the immobilized structure^[14] or intermolecular π -stacking.^[15] Furthermore, model compounds were designed and synthesized to investigate fundamental electronic features like conductance,^[16] rectification^[17] and switching.^[18,19] The development of suitable molecular systems and integration platforms will contribute to both fundamental science and future technological innovations.

Among the basic electronic functions that have to be transferred to a molecular level, bistable switching is particularly interesting as the fundamental basis of molecule-based memory devices.^[1] A molecule-based device that can be toggled between two distinct conductance states on demand, usually under the control of an external stimulus (e.g. electrical, electrochemical, optical), is called a molecular switch. For example, photoswitchable dithienylethynes^[20] and electrochemically addressable viologens^[21–23] and perylenes^[24] have been investigated in a mechanically controlled break junction (MCBJ) and in a scanning tunneling microscopy (STM) set-up, respectively. A molecular rod comprising a central 6,6'-dinitro-2,2'-bipyridine unit^[25,26] and interlocked supermolecules^[27] displayed hysteretic switching properties. Negative differential resistance (NDR) effects have been observed for a nitro-functionalized oligo(phenylene ethynylene) (OPE) rod in laterally limited SAMs.^[28]

Under electrochemical control, viologen derivatives show potential-dependent single-molecule transport properties.^[21,22] Furthermore, anthraquinone^[29] and tetrathiafulvalene^[30] redox chromophores have been integrated into OPE rods. The oxidation state of the redox-active element is expected to control the extent of electronic delocalization and thus the electronic transparency of such systems. Indeed, quinone-containing OPE structures showed NDR phenomena in SAMs investigated by STM.^[31] More recently, reversible conductance switching has been found for

[a] Department of Chemistry, University of Basel, St. Johanns-Ring 19, 4056 Basel, Switzerland
E-mail: marcel.mayor@unibas.ch

[b] Department of Chemistry and Biochemistry, University of Bern, Freiestrasse 3, 3012 Bern, Switzerland
E-mail: thomas.wandlowski@dcf.unibe.ch

[c] Institute for Nanotechnology, Forschungszentrum Karlsruhe GmbH, P.O. Box 3640, 76021 Karlsruhe, Germany

quinone-based oligo(phenylene vinylene) molecules using electrochemical STM.^[32]

We previously described the synthesis and the electrochemical behaviour of a linear molecular rod based on a OPE backbone equipped with a redox-active catechol subunit.^[33] Gold–molecule–gold junctions were formed with the corresponding dimethyl-protected rod in a STM-based set-up, and single-molecule transport investigations revealed a set of three conductance values varying over two orders of magnitude. In this context, our current interest is focused on the integration of such a catechol-based rod into more complex macrocyclic structures as potential compounds to investigate redox-state-dependent transport properties arising from conformational changes in the future.

Results and Discussion

Herein we report the synthesis of the macrocyclic rod **1** from well-designed building blocks. Spectroscopic and electrochemical investigations were carried out to question the redox activity of the integrated catechol subunit in **1**. In preliminary experiments, the macrocycle **1** was immobilized in Au–I'–Au junctions using a STM set-up to investigate the first transport features through the macrocycle structure and to corroborate the suitability of the proposed structure as a functional unit in a molecular device.

Molecular Design

The macrocyclic rod **1**, a structural analog of a previously reported nitro-functionalized macrocycle,^[19] consists of five ethynyl-linked phenyl rings (Figure 1, A). The linear rod substructure comprises both sulfur-function-

alized phenyl rings and the central catechol unit. The latter is redox-active and profits from freedom of rotation along the linear rod axis. The terminal acetyl-protected sulfur groups act as anchor groups dedicated to the immobilization of the macrocycle between a pair of gold electrodes. Their *para* positioning with respect to the linear rod ensures a rather strong coupling of the linear rod substructure with the electronic levels of the electrodes.^[12]

Both terminal units are further connected to the bridging handle made of the two lateral ethynyl-linked phenyl rings. The bridging substructure itself is poorly conjugated owing to the *meta* substitution of each of its phenyl rings. In addition, the handle is linked to the terminal units at the weakly coupled *meta* position to the sulfur anchor groups.^[12] Thus, after immobilization of the macrocycle between gold electrodes, the current through the strongly conjugated linear rod is expected to be predominant while the contribution of leaking currents through the bridging handle should be minimized. The bridging substructure plays two roles. Firstly, it inhibits the rotation of the terminal units by locking them in a planar conformation. Secondly, it provides the phenyl rings of the handle in the vicinity of the catechol unit for additional intramolecular interactions.

The electronic transparency of the linear rod is expected to depend on the torsion angle given by the relative rotational position of the central catechol unit with respect to the plane of the macrocycle. After formation of a gold–molecule–gold junction, the macrocycle structure should attain a fixed conformation due to a pair of intramolecular hydrogen bonds between the oxygen atoms of the catechol and the facing hydrogen atoms of the handle (Figure 1, B, left side). Indeed, the *sp*³ hybridization of the lone-pairs of the catechol oxygen atoms should allow to reach such a favorable conformation in which the central catechol subunit is only slightly distorted from planarity. By consider-

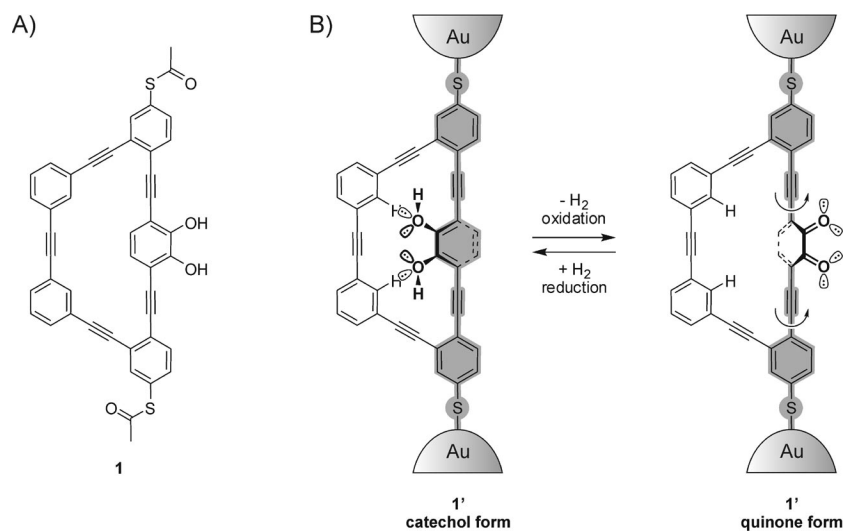


Figure 1. A) Target macrocyclic rod **1**. B) Redox chemistry of the macrocyclic rod **1'** after immobilization between gold electrodes. Intramolecular hydrogen bonds are only possible for the catechol form favoring an only slightly tilted fixed position of the revolving subunit. The lone-pairs of the oxygen atoms are displayed to visualize the geometrical argument. The extent of electronic delocalization along the linear rod is highlighted in grey.

ably planarizing the linear rod embedded between both electrodes, an increased conjugation is expected to enlarge the systems electronic transparency (high conductance state). Upon oxidation, the catechol moiety is converted into the corresponding quinone (Figure 1, B, right side). Already the alteration of the oxidation state of the central unit might alter the electronic transparency of the system. However, as both redox states comprise a fully conjugated π -backbone, the extent of this effect will remain limited in an electrochemical experiment. Furthermore, the comparison with already reported model systems consisting exclusively of the macrocycle's rod subunit^[33] will enable to allocate this contribution precisely. In the oxidized quinone form, the sp^2 -hybridized lone-pairs are no longer pointing towards the *endo*-annular hydrogen atoms of the macrocycle's handle and thus, the formation of intermolecular hydrogen bonds is not possible. The central quinone subunit is thus expected to revolve freely around the linear rod axis providing an averaged transport signal (low conductance state). In particular conformations with an almost perpendicular central quinone subunit are expected to considerably reduce the electronic transparency of the linear rod by restricting the π -electron delocalization. Theoretical calculations predict a decrease in the transport current for such a perpendicular arrangement.^[34–37] Therefore, the immobilized macrocyclic rod **1'** is expected to behave like a bistable switch exhibiting two distinct conductance states arising from a reversible two-electron two-proton electrochemical process.

Owing to their unique properties, shape-persistent macrocycles are at the forefront attention as rigid supramolecular building blocks for organic materials.^[38–41] The concept of integrating a revolving unit into a macrocyclic phenylacetylene framework has already been achieved in turnstile structures.^[42] A comparable turnstile motif provided a bicyclic host with allosteric anion binding properties.^[43]

Synthetic Strategy

The macrocyclic rod **1** was synthesized according to a strategy that previously allowed the stepwise assembly of

closely related macrocyclic structures (Figure 2).^[19] The assembly profits from the reported accessibility of intermediates **2**, **3** and **4**.^[19] The synthesis of 5-(*tert*-butylsulfanyl)-2-nitrophenyl trifluoromethanesulfonate **2** starts off with commercially available 5-fluoro-2-nitrophenol and involves the four-step sequence: (i) protection of the phenol, (ii) substitution of the fluorine atom with sodium *tert*-butylthiolate, (iii) deprotection of the phenol, (iv) formation of the triflate by reaction with triflic anhydride (50% yield). 3,3'-Bis(ethynyl)tolane **3** is easily obtained from commercially available 1-bromo-3-iodobenzene in three steps (77% yield).

Using palladium- and copper-catalyzed Sonogashira reaction conditions, the triflate **2** and diacetylene **3** are then coupled to harness the bridging handle with the anchor units prior to the reduction of the nitro groups. Subsequent twofold diazotization and Sandmeyer reaction affords the advanced intermediate **4** in 32% yield from **3**. Compound **4** bears two iodines known as excellent leaving groups for Sonogashira cross-coupling reactions. Based on the results obtained during the assembly of the previously reported nitro-functionalized macrocycle,^[19] only a stepwise assembly strategy for the macrocycle **6** with the diiodo compound **4** and the monoprotected diacetylene **5** was considered. Finally, protection group chemistry should allow to transprotect the terminal sulfur groups and to provide the desired central catechol subunit.

Synthesis

The synthesis of the newly developed building block **5**, the assembly of the macrocyclic precursor **6** comprising a masked catechol subunit and *tert*-butyl-protected sulfur groups, and the final tandem catechol deprotection/sulfur transprotection step yielding the target macrocyclic rod **1** are described here.

Compound **5** is made of an orthoformate-protected catechol ring decorated with one TIPS-protected and one free terminal acetylene unit (Scheme 1). Ethyl orthoformate is a versatile catechol protecting group with a large variety of potential deprotecting reagents ranging from strong Lewis acids like boron tribromide to mild acids like acetic acid.^[33]

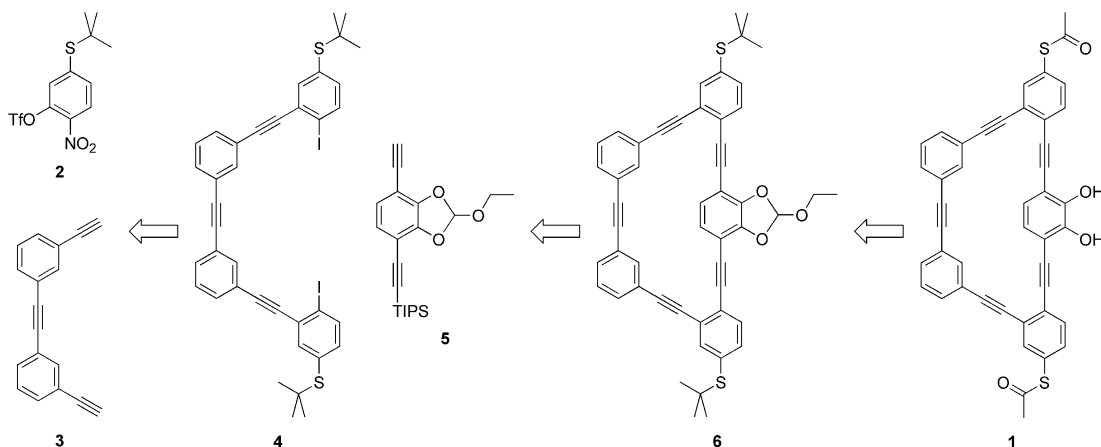
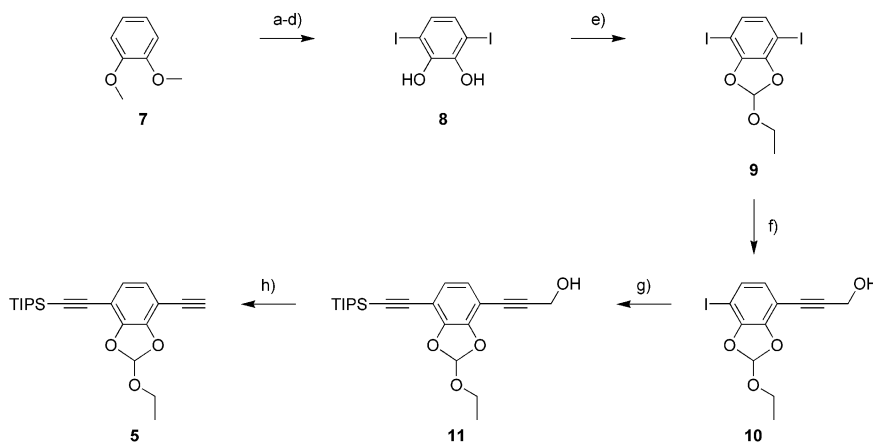


Figure 2. Retrosynthetic strategy to assemble the macrocyclic rod **1** from suitable building blocks.



Scheme 1. Synthesis of the monoprotected diacetylene **5**. a) 1. *n*BuLi, TMEDA, hexane, room temp., 2. TMSCl, -78°C to room temp., 85%; b) 1. *n*BuLi, TMEDA, hexane, 0°C to room temp., 2. TMSCl, -78°C to room temp., 89%; c) ICl, CH_2Cl_2 , 0°C to room temp., 81%; d) BBr_3 , CH_2Cl_2 , -78°C to room temp., 90%; e) $\text{CH}(\text{OEt})_3$, Amberlyst 15, toluene, reflux, 62%; f) propargyl alcohol, $\text{Pd}(\text{PPh}_3)_2\text{Cl}_2$, CuI, *i*Pr₂NH, THF, room temp., 71%; g) (triisopropylsilyl)acetylene, $\text{Pd}(\text{PPh}_3)_2\text{Cl}_2$, CuI, *i*Pr₂NH, THF, room temp., 90%; h) MnO_2 , KOH, CH_2Cl_2 , room temp., 78%.

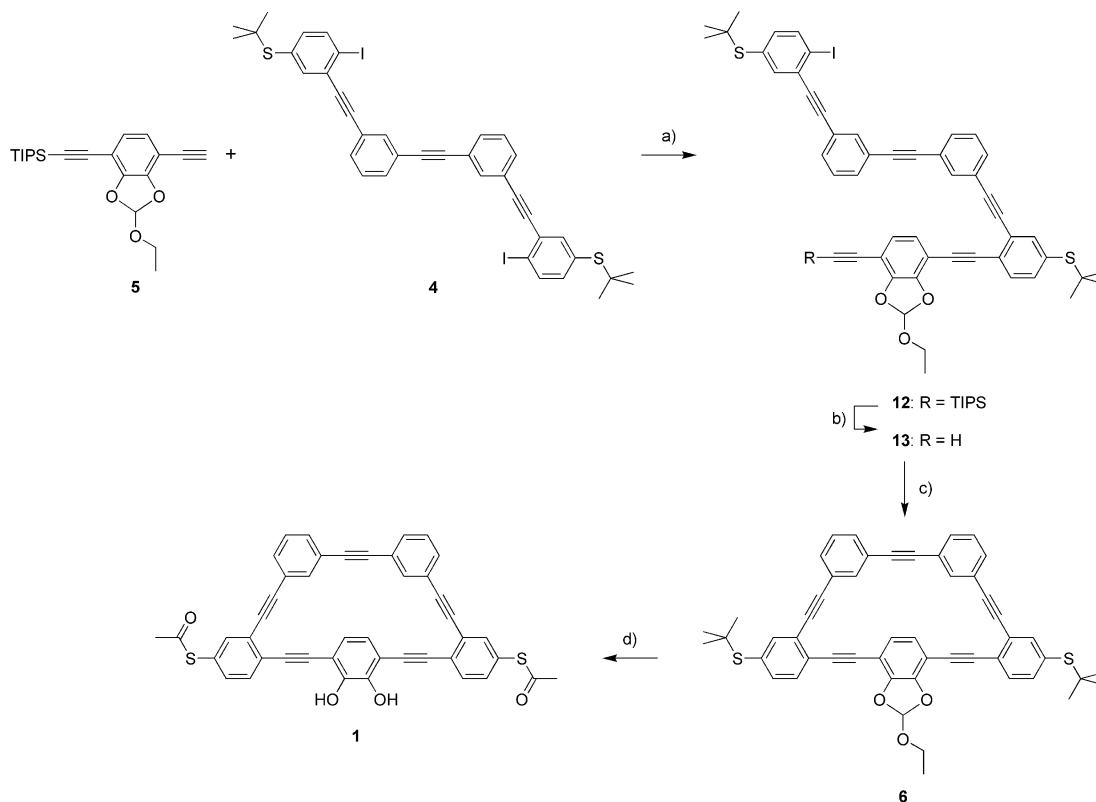
Firstly, commercially available 1,2-dimethoxybenzene (veratrole) **7** was converted into the diiodocatechol **8** in four steps (55% yield) according to a previously reported procedure.^[44] A repeated sequence of monolithiation followed by reaction with trimethylsilyl chloride allowed the stepwise introduction of two TMS groups onto the dimethoxybenzene ring. Iodo-desilylation with iodine monochloride led to 1,4-diiodo-2,3-dimethoxybenzene which finally gave the diiodocatechol **8** by demethylation with boron tribromide. The diiodo orthoester **9** was then obtained by condensation of **8** with triethyl orthoformate in refluxing toluene in presence of Amberlyst 15 resin as acidic catalyst (62% yield).^[33]

The formation of the monoprotected diacetylene **5** from the diiodo intermediate **9** was inspired by an elegant approach using orthogonal acetylene protecting groups with different polarities.^[45] The diiodo orthoester **9** was thus subjected to a Pd- and Cu-catalyzed cross-coupling reaction with 0.69 equiv. of propargyl alcohol. A mixture of the unreacted diiodo starting material **9**, the desired monosubstitution product **10** and disubstitution product 2,3-(ethoxymethylenedioxy)-1,4-bis(3-hydroxyprop-1-ynyl)benzene as minor by-product was obtained. The significant influence of the hydroxymethyl group on the R_f values of the products led to the straightforward isolation of **10** by column chromatography in 71% yield. It is worth mentioning that the reaction could then be repeated with the recovered diiodo orthoester **9** (23%). Next, the monoiodo compound **10** readily reacted with TIPS-acetylene in classical Sonogashira reaction conditions to give the intermediate **11** bearing two different acetylene protecting groups. Treatment of compound **11** with activated manganese dioxide and potassium hydroxide in dichloromethane at room temperature^[46] promoted the selective cleavage of the hydroxymethyl moiety by oxidation/decarbonylation and the formation of the monoprotected diacetylene **5** in 78% yield. Again, the combination of the non-polar TIPS group and the polar hydroxymethyl group allowed the efficient isolation of the desired building block **5**.

To assemble the macrocycle structure, the protocol reported for the nitro-functionalized macrocycle was applied.^[19] Compound **5** was added dropwise to an excess of diiodo intermediate **4** (2.9 equiv.) in presence of catalytic amounts of $\text{Pd}(\text{PPh}_3)_2\text{Cl}_2$ and CuI to afford the monosubstituted derivative **12** in 66% yield (Scheme 2). Deprotection of the TIPS-protected acetylene **12** with tetrabutylammonium fluoride led almost quantitatively to the free acetylene compound **13** bearing one iodo group. This difunctionalized open-ring oligomer was then subjected to a macrocyclization reaction in a highly diluted (10^{-4} M) toluene solution containing one equivalent of $\text{Pd}(\text{PPh}_3)_4$, one equivalent of CuI and diisopropylethylamine as a base. High-dilution reaction conditions and stoichiometric amounts of palladium and copper were used to favor the desired intramolecular ring closure over the intermolecular reactions leading to oligomeric by-products. Thus, the macrocycle **6** was obtained in a fair yield of 42% after column chromatography.

Finally, the transprotection of *S*-tert-butyl groups into *S*-acetyl groups as well as the catechol deprotection steps remained. Interestingly, boron tribromide is reported as a suitable reagent for both purposes.^[33] To our satisfaction, the target macrocyclic rod **1** was successfully obtained in 64% yield by concomitant catechol deprotection and terminal sulfur transprotection by use of an excess of boron tribromide (10 equiv.) in toluene containing acetyl chloride at room temperature. The catechol-based macrocycle **1** displays reasonable thermal stability in contrast to the previously described nitro-functionalized macrocycle.^[19]

All the new compounds were fully characterized by conventional analytical and spectroscopic techniques like ^1H and ^{13}C NMR spectroscopy and mass spectrometry. Furthermore, the purity of the compounds was confirmed by elemental analysis. In order to gain additional structural details, numerous attempts to grow single crystals from the macrocyclic structure were made. Finally, single crystals of compound **6** suitable for X-ray analysis were obtained by



Scheme 2. Synthesis of the macrocyclic rod **1**. a) Pd(PPh₃)₂Cl₂, CuI, *i*Pr₂NH, THF, room temp., 66%; b) TBAF, AcOH, THF, room temp., 95%; c) Pd(PPh₃)₄, CuI, *i*Pr₂NEt, toluene, room temp., 42%; d) BBr₃, AcCl, toluene, room temp., 64%.

slow evaporation of a solution of **6** in a mixture of dichloromethane and hexane. The subsequently solved solid-state structure of **6** is displayed in Figure 3. The intramolecular sulfur-to-sulfur distance is 20.098 Å and the average C–C bond length of the acetylene bridges is 1.197 Å. The central orthoformate-protected catechol ring is twisted with a torsion angle of 25.00° with respect to the mean plane of the macrocycle comprising the four other phenyl rings. Remarkably, the average distance between the catechol oxygen atoms and the facing hydrogen atoms of the handle is 2.451 Å, pointing at a fixed arrangement of the protected central catechol subunit due to two intermolecular hydro-

gen bonds. It is noteworthy that a comparable conformation will also be expected for the on-state of the integrated macrocycle.

UV/Vis Absorption

The linear rod **14**^[33] (Figure 4) was used as a reference compound for the spectroscopic and electrochemical studies. It is based on a central catechol unit implemented into a rod-like OPE structure capped with acetylsulfanyl end groups. Thus, it is identical to the linear rod substructure of the macrocyclic rod **1** lacking the bridging handle.

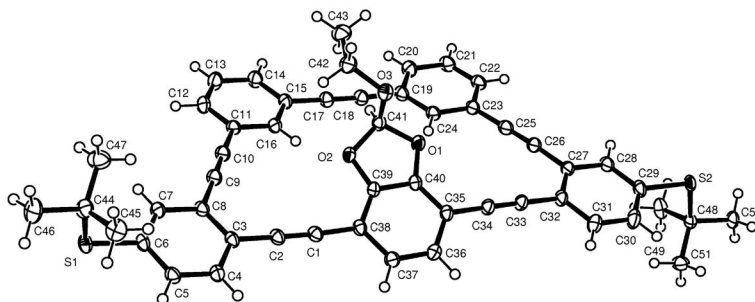


Figure 3. X-ray structure of the protected macrocyclic rod **6** (ORTEP, thermal ellipsoids set at the 50% probability level). Selected bond lengths [Å] and angles [°]: S(1)–C(44) 1.8571(13), S(1)–C(6) 1.7713(11), S(2)–C(48) 1.8689(13), S(2)–C(29) 1.7718(13), C(1)–C(2) 1.1970(16), C(9)–C(10) 1.1963(18), C(17)–C(18) 1.2006(17), C(25)–C(26) 1.1962(19), C(33)–C(34) 1.1973(16), O(1)–C(40) 1.3819(14), O(1)–C(41) 1.4165(14), O(2)–C(39) 1.3789(15), O(2)–C(41) 1.4417(15), O(3)–C(41) 1.3768(15), O(3)–C(42) 1.4556(15), C(6)–S(1)–C(44) 102.69(6), C(29)–S(2)–C(48) 102.68(6), C(41)–O(3)–C(42) 112.37(10).

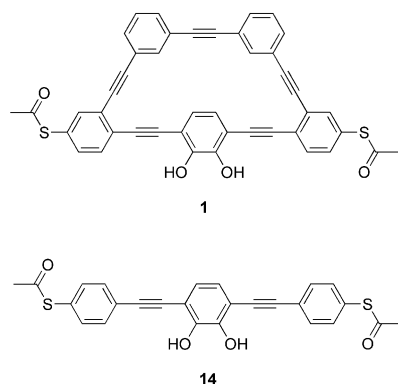


Figure 4. Structure of the reference linear rod **14** lacking the bridging handle present in the macrocyclic rod **1**.

UV/Vis absorption spectra of compounds **14**, **1**, **6** and catechol were measured in dichloromethane at room temperature (Figure 5, Table 1). As a linear Lambert-Beer-like concentration dependence of the UV/Vis signal of **1** was observed in the investigated concentration range (0.3–10 μM solutions), the obtained UV/Vis spectra were attributed to freely dissolved species and aggregation of the macrocyclic structure was excluded at these concentrations in CH_2Cl_2 . Upon integration of the catechol ring into the linear and macrocyclic rods (**14** and **1**, respectively), the absorption maximum λ_{max} undergoes a striking bathochromic and hy-

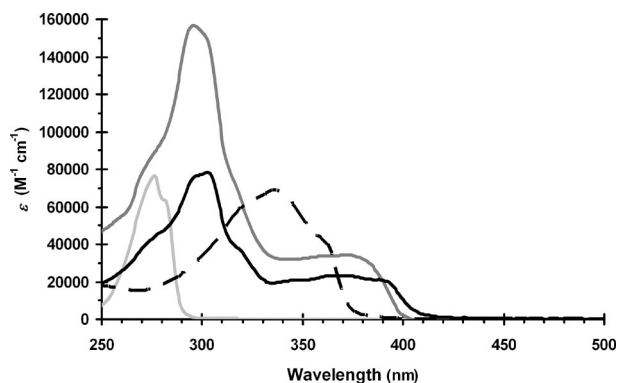


Figure 5. UV/Vis absorption spectra of catechol (light gray, magnification 30 \times), linear rod **14** (dashed), free catechol macrocyclic rod **1** (black) and orthoformate-protected macrocyclic rod **6** (dark gray) in CH_2Cl_2 .

perchromic shift, reflecting the extended π -electron delocalization over these conjugated structures. The absorption profiles of the orthoformate-protected and free catechol macrocycles (**6** and **1**, respectively) are quite comparable to those of oligomers with alternating *ortho*- and *para*-(phenylene ethynylene) backbones.^[47,48] This also reflects the π -conjugation disruption by the *meta* branching in the lateral handle. In particular, the absorption maximum of the macrocyclic rod **1** appears at 303 nm while its lowest energy absorption band spreads beyond 400 nm.

Electrochemistry

The electrochemical properties of compounds **14**, **1**, **6** and catechol were investigated in a 1:1 mixture of methanol and dichloromethane containing 0.15 M sodium acetate as the supporting electrolyte using a glassy carbon electrode (Figure 6, Table 1). The macrocyclic rod **1** reveals an anodic wave at +125 mV assigned to the oxidation of the catechol unit to the corresponding quinone form. On the reverse scan, a cathodic peak appears at +32 mV upon reduction of the newly formed quinone and regeneration of the initial catechol. Thus, a quasi-reversible process is found for the catechol/quinone couple in **1**. This behaviour is pretty similar to the one previously observed for the linear rod **14**.^[33] A decrease in the electrochemical response of the system

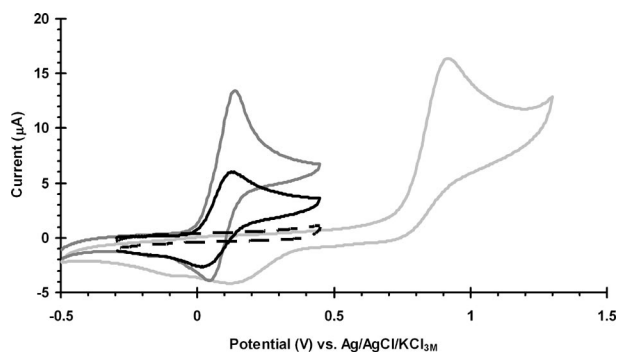


Figure 6. Cyclic voltammograms of 1 mM solutions of catechol (light gray), linear rod **14** (dark gray), free catechol macrocyclic rod **1** (black) and orthoformate-protected macrocyclic rod **6** (dashed) in $\text{MeOH}/\text{CH}_2\text{Cl}_2$ (1:1) at a glassy carbon electrode. Supporting electrolyte: 0.15 M NaOAc. Scan rate: 100 mV s^{-1} .

Table 1. Spectroscopic and electrochemical properties of catechol, linear rod **14**, free catechol macrocyclic rod **1** and orthoformate-protected macrocyclic rod **6**.

Compound	Spectroscopic properties ^[a]			Electrochemical properties ^[b]		
	λ_{max} [nm]	ϵ_{max} [$\text{M}^{-1} \text{cm}^{-1}$]	E_{gap} [eV] ^[c]	E_{ox} [mV]	E_{red} [mV]	ΔE [mV]
Catechol	276	2 550	4.26	906	129	777
Linear rod 14	336	68 600	3.29	135	51	84
Macrocyclic rod 1	303	78 300	3.05	125	32	93
Protected macrocycle 6	296	156 600	3.13	–	–	–

[a] In CH_2Cl_2 solution. [b] In $\text{MeOH}/\text{CH}_2\text{Cl}_2$ (1:1) solution at a glassy carbon electrode. Supporting electrolyte: 0.15 M NaOAc. Scan rate: 100 mV s^{-1} . [c] HOMO–LUMO energy gap determined optically from the absorption onset corresponding to the wavelength at which ϵ is 5% of ϵ_{max} .

after each cycle has been observed, which is most likely attributed to a partial blocking of the electrode due to adsorption.

Interestingly, the greatly facilitated oxidation of **1** in comparison with catechol (0.78 V shift to more negative potentials) corroborates the beneficial impact of π -conjugation on the HOMO–LUMO energy gap (E_{gap}), as observed by UV/Vis spectroscopy (Figure 5, Table 1). Owing to the orthoformate protecting group masking its catechol moiety, macrocycle **6** shows no redox activity in the same potential range.

Comparison of the electrochemical properties of the orthoformate-protected and free catechol macrocycles (**6** and **1**, respectively) demonstrates that the deprotected catechol is the origin of the observed redox activity. Clearly, the catechol subunit integrated into the macrocyclic rod **1** provides a quasi-reversible two-electron two-proton process in a protic medium such as methanol even more easily than the parent unfunctionalized catechol.

Single-Molecule Conductance Measurements

A modified STM-based break junction technique was employed to measure the single-junction conductances of the macrocyclic and linear rods (**1** and **14**, respectively) covalently attached by thiol linkers to two gold electrodes.^[49] The experiments were carried out in a 25 μM solution of **1** or **14** in a 4:1 mixture of mesitylene and THF. The method is based on the repeated formation and breaking of individual and small groups of metal–molecule–metal junctions.

As an example, Figure 7 shows individual conductance curves which exhibit a series of plateaus and steps. The plateaus are well developed despite the fact that they appear relatively noisy. These conductance steps are attributed to the bridging of single or integer numbers of the OPE-type molecules in the junction. The statistical analysis of these data leads to the construction of conductance histograms (see Exp. Sect. for details).^[49] There is a certain variation in the magnitude and the shape of the conductance steps from one molecular junction to another, as reflected in the spread and asymmetry of the histogram, which most probably represents different microscopic details of the individual junctions. However, all conductance histograms, typically constructed from 300 to 600 curves (out of 3000), showed a pronounced peak at $G = (1.7 \pm 0.4) \times 10^{-4} G_0$ (13 ± 3 nS) (Figure 8, A) and $G = (1.5 \pm 0.2) \times 10^{-4} G_0$ (12 ± 2 nS) (Figure 8, B) for **1** and **14**, respectively. It is noteworthy that sharply abrupt or exponentially decaying (60–70%) and very noisy (10–20%) conductance traces were not considered in the construction of the histograms. The pronounced tail region towards higher conductance values may reflect the “blurred” contribution of multimolecular junctions, which appear to be rather typical for rigid rod-type molecules with thiol anchoring groups.^[16]

The conductance values of the macrocyclic rod **1** and the reference linear rod **14** are identical within the error limit of the experiment. This comparison demonstrates that the

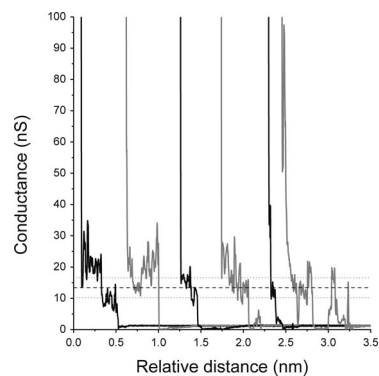


Figure 7. Typical single-molecule conductance traces of the macrocycle **1** attached to two gold electrodes ($V_{\text{bias}} = 0.10$ V).

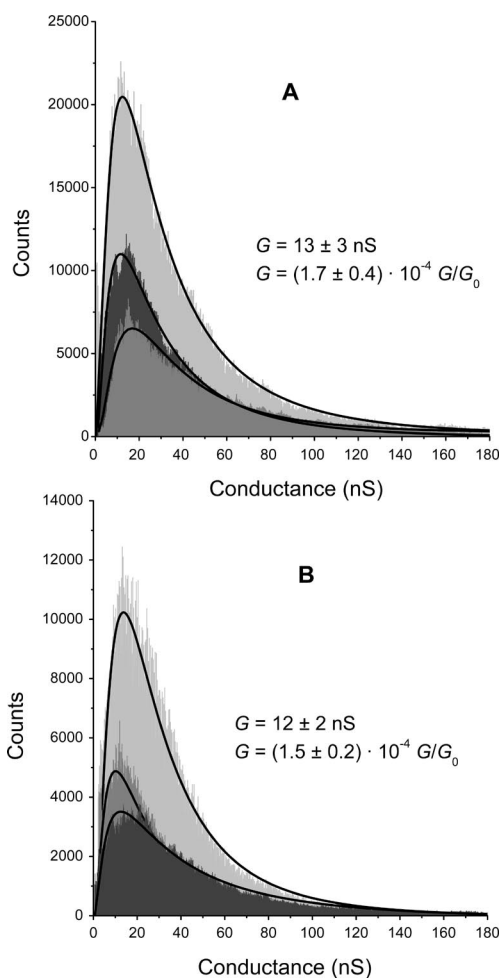


Figure 8. Plateau-point histograms of the macrocyclic rod **1** (A) and the linear rod **14** (B) for various bias voltages: 0.065 (dark gray), 0.10 (light gray) and 0.17 V (medium gray).

side loop in **1** does not modify, under present experimental conditions, the junction conductance of the OPE rod. Furthermore, no evidence was found for junctions with distinctly different coordination geometries of the terminal sulfur–gold bonds. Interestingly, the conductance values of compounds **1** and **14** are of similar order of magnitude as those measured for the unsubstituted OPE rod employing

Tao's STM-based approach^[50] or a mechanically controlled break junction.^[16] The authors of the latter paper also demonstrated that the asymmetric tail in the descending region of the conductance histogram might reflect overlapping contributions from junctions with one, two, or a multiple of molecules bridging the gap in parallel.

Conclusions

The synthesis of a novel redox-active macrocyclic rod **1** comprising a catechol subunit has been achieved by applying a previously developed assembly strategy. Notably, the ethyl orthoformate protected catechol subunit enabled not only the integration of the electrochemically active subunit into the molecular framework of the macrocycle, but also its concerted deprotection and transprotection of the sulfur anchoring groups. The residual redox activity of catechol moiety integrated into **1** was demonstrated by cyclic voltammetry investigations. Furthermore, molecular junctions (Au-1'-Au) were successfully formed in a STM-based setup and analyzed statistically, showing the suitability of the macrocyclic rod **1** for single-molecule transport investigations. Similar single-molecule conductance values were found for the macrocyclic and linear rods (**1** and **14**, respectively), confirming the weak electronic coupling of the bridging handle in **1**.

STM-based conductance measurements in an electrochemically controlled environment are currently in progress to evaluate the hypothesized switching mechanism arising from redox-state-dependent conformational changes. In addition, the macrocycle structure is being optimized in order to enhance the ability of the macrocyclic rod to form intramolecular hydrogen bonds.

Experimental Section

General Methods: All solvents and chemicals were of analytical grade and were used as supplied without further purification. Flash chromatography was performed on Fluka silica gel 60 (0.040–0.063 mm). ¹H (400 MHz) and ¹³C (100 and 125 MHz) NMR spectra were recorded at room temperature using the residual proton resonances in deuterated solvents as internal references. Chemical shifts (δ) are reported in ppm. Mass spectra were obtained by electron-impact (EI) or fast atom bombardment (FAB) mass spectrometry. All mixtures of solvents are given in v/v ratio.

3-(2-Ethoxy-7-iodo-1,3-benzodioxol-4-yl)prop-2-yn-1-ol (10): Propargyl alcohol (55 μ L, 0.94 mmol) was added to a degassed solution of 2-ethoxy-4,7-diiodo-1,3-benzodioxole (**9**) (567 mg, 1.36 mmol), Pd(PPh₃)₂Cl₂ (19 mg, 0.03 mmol) and CuI (10 mg, 0.05 mmol) in a mixture of THF (10 mL) and *i*Pr₂NH (2 mL). The resulting solution was stirred at room temp. overnight and the solvents were evaporated. CH₂Cl₂ and H₂O were added, the organic phase was separated and the aqueous phase was further extracted with CH₂Cl₂. The combined organic layers were dried with MgSO₄, filtered and the solvents evaporated to dryness. Flash chromatography (SiO₂, CH₂Cl₂/MeOH, 100:0 to 99:1) afforded starting material **9** (132 mg, 23%) and product **10** (231 mg, 71%) as a yellow oil. *R*_f = 0.28 (SiO₂, CH₂Cl₂/MeOH, 99:1). ¹H NMR (400 MHz, CDCl₃): δ = 1.27 (t, ³*J*_{H,H} = 7.2 Hz, 3 H, CH₃), 2.50 (br. s, 1 H,

OH), 3.74 (q, ³*J*_{H,H} = 7.2 Hz, 2 H, OCH₂), 4.49 (br. s, 2 H, CH₂), 6.66 (d, ³*J*_{H,H} = 8.4 Hz, 1 H), 6.95 (s, 1 H, OCH), 7.08 (d, ³*J*_{H,H} = 8.4 Hz, 1 H) ppm. ¹³C NMR (100 MHz, CDCl₃): δ = 14.8 (CH₃), 51.6 (CH₂OH), 60.0 (OCH₂), 71.0, 78.8 (C \equiv C), 92.8 (C \equiv C), 104.0, 118.7 (OCH), 126.4, 130.1, 145.8 (OC), 147.7 (OC) ppm. C₁₂H₁₁IO₄ (346.12): calcd. C 41.64, H 3.20; found C 41.73, H 3.33. MS (EI): *m/z* (%) = 346.9 (100) [M]⁺, 300.9 (57) [M - C₂H₅O]⁺, 271.9 (77) [M - C₃H₆O₂]⁺.

3-{2-Ethoxy-7-[(triisopropylsilyl)ethynyl]-1,3-benzodioxol-4-yl}prop-2-yn-1-ol (11): (Triisopropylsilyl)acetylene (820 μ L, 3.55 mmol) was added to a degassed solution of compound **10** (1.026 g, 2.96 mmol), Pd(PPh₃)₂Cl₂ (104 mg, 0.15 mmol) and CuI (28 mg, 0.15 mmol) in a mixture of THF (60 mL) and *i*Pr₂NH (10 mL). The resulting solution was stirred at room temp. overnight and the solvents were evaporated. CH₂Cl₂ and H₂O were added, the organic phase was separated and the aqueous phase was further extracted with CH₂Cl₂. The combined organic layers were dried with MgSO₄, filtered and the solvents evaporated to dryness. Flash chromatography (SiO₂, CH₂Cl₂/MeOH, 100:0 to 99:1) afforded **11** (1.066 g, 90%) as a yellow oil. *R*_f = 0.32 (SiO₂, CH₂Cl₂/MeOH, 99:1). ¹H NMR (400 MHz, CDCl₃): δ = 1.10–1.14 [m, 21 H, SiCH(CH₃)₂], 1.28 (t, ³*J*_{H,H} = 7.0 Hz, 3 H, CH₃), 1.98 (br. t, ³*J*_{H,H} = 5.8 Hz, 1 H, OH), 3.76 (qd, ³*J*_{H,H} = 7.1, ⁴*J*_{H,H} = 2.0 Hz, 2 H, OCH₂), 4.52 (br. d, ³*J*_{H,H} = 6.0 Hz, 2 H, CH₂), 6.83 (d, ³*J*_{H,H} = 8.4 Hz, 1 H), 6.88 (d, ³*J*_{H,H} = 8.4 Hz, 1 H), 6.96 (s, 1 H, OCH) ppm. ¹³C NMR (100 MHz, CDCl₃): δ = 11.3 (SiCH), 15.0 (CH₃), 18.7 (CH₃), 51.8 (CH₂OH), 59.9 (OCH₂), 79.5 (C \equiv C), 93.1 (C \equiv C), 97.8 (C \equiv C), 100.0 (C \equiv C), 103.9, 105.5, 119.7 (OCH), 124.7, 125.3, 147.1 (OC), 147.4 (OC) ppm. C₂₃H₃₂O₄Si (400.58): calcd. C 68.96, H 8.05; found C 68.62, H 7.96 MS (EI): *m/z* (%) = 400.3 (16) [M]⁺, 357.2 (29) [M - C₃H₇]⁺, 311.2 (15) [M - CH₃O - C₃H₆O]⁺, 283.2 (100) [M - CH₃O - 2 C₃H₇]⁺, 241.1 (14) [M - C₃H₆O₂ - 2 C₃H₇]⁺.

[(2-Ethoxy-7-ethynyl-1,3-benzodioxol-4-yl)ethynyl](triisopropyl)silane (5): Activated MnO₂ (4.36 g, 42.6 mmol) and powdered KOH (1.39 g, 21.3 mmol) were added in four equal portions over 4 h to a degassed solution of compound **11** (1.066 g, 2.66 mmol) in CH₂Cl₂ (120 mL). The resulting suspension was stirred at room temp. overnight. After filtration, the solvent was evaporated. Flash chromatography (SiO₂, hexane/CH₂Cl₂, 80:20) afforded **5** (768 mg, 78%) as a yellow oil. *R*_f = 0.36 (SiO₂, hexane/CH₂Cl₂, 70:30). ¹H NMR (400 MHz, CDCl₃): δ = 1.10–1.14 [m, 21 H, SiCH(CH₃)₂], 1.29 (t, ³*J*_{H,H} = 7.2 Hz, 3 H, CH₃), 3.34 (s, 1 H, \equiv CH), 3.77 (qd, ³*J*_{H,H} = 7.1, ⁴*J*_{H,H} = 1.1 Hz, 2 H, OCH₂), 6.87 (s, 2 H, 5-H, 6-H), 6.98 (s, 1 H, OCH) ppm. ¹³C NMR (100 MHz, CDCl₃): δ = 11.4 (SiCH), 15.0 (CH₃), 18.7 (CH₃), 59.9 (OCH₂), 77.5 (C \equiv C), 82.9 (C \equiv C), 97.9 (C \equiv C), 100.0 (C \equiv C), 103.4, 105.8, 119.9 (OCH), 124.9, 125.2, 147.5 (OC), 147.7 (OC) ppm. C₂₂H₃₀O₃Si (370.56): calcd. C 71.31, H 8.16; found C 71.56, H 8.24. MS (EI): *m/z* (%) = 370.2 (31) [M]⁺, 327.1 (100) [M - C₃H₇]⁺, 299.1 (10) [M - C₃H₇ - C₂H₅ + H]⁺, 271.1 (50) [M - C₃H₇ - C₃H₆O + 2 H]⁺.

[(7-{[4-(*tert*-Butylsulfanyl)-2-({3-[(3-{5-(*tert*-butylsulfanyl)-2-iodophenyl]ethynyl}phenyl)ethynyl]phenyl]ethynyl}phenyl]ethynyl]-2-ethoxy-1,3-benzodioxol-4-yl)ethynyl](triisopropyl)silane (12): A degassed solution of compound **5** (63 mg, 0.17 mmol) in THF (5 mL) was added dropwise to a degassed solution of compound **4** (404 mg, 0.50 mmol), Pd(PPh₃)₂Cl₂ (6 mg, 8.55 μ mol) and CuI (3 mg, 15.8 μ mol) in a mixture of THF (40 mL) and *i*Pr₂NH (8 mL). The resulting solution was stirred at room temp. overnight and the solvents were evaporated. Flash chromatography (SiO₂, hexane/CH₂Cl₂, 80:20) afforded **12** (117 mg, 66%) as a white solid; m.p. 85–86 °C. *R*_f = 0.26 (SiO₂, hexane/CH₂Cl₂, 70:30). ¹H NMR (400 MHz, CDCl₃): δ = 1.10–1.14 [m, 21 H, SiCH(CH₃)₂], 1.23 (t,

$^3J_{\text{H,H}} = 7.0$ Hz, 3 H, CH₃), 1.31 [s, 9 H, C(CH₃)₃], 1.33 [s, 9 H, C(CH₃)₃], 3.70 (q, $^3J_{\text{H,H}} = 7.1$ Hz, 2 H, OCH₂), 6.92 (d, $^3J_{\text{H,H}} = 8.8$ Hz, 1 H), 6.97(1) (s, 1 H, OCH), 6.97(3) (d, $^3J_{\text{H,H}} = 7.6$ Hz, 1 H), 7.16 (dd, $^3J_{\text{H,H}} = 8.0$, $^4J_{\text{H,H}} = 2.0$ Hz, 1 H), 7.36 (t, $^3J_{\text{H,H}} = 7.8$ Hz, 1 H), 7.38 (t, $^3J_{\text{H,H}} = 8.2$ Hz, 1 H), 7.48 (dd, $^3J_{\text{H,H}} = 8.0$, $^4J_{\text{H,H}} = 1.6$ Hz, 1 H), 7.50–7.60 (m, 5 H), 7.68 (d, $^4J_{\text{H,H}} = 2.4$ Hz, 1 H), 7.74 (d, $^4J_{\text{H,H}} = 1.6$ Hz, 1 H), 7.78 (t, $^4J_{\text{H,H}} = 1.4$ Hz, 1 H), 7.80 (t, $^4J_{\text{H,H}} = 1.6$ Hz, 1 H), 7.83 (d, $^3J_{\text{H,H}} = 8.0$ Hz, 1 H) ppm. ¹³C NMR (100 MHz, CDCl₃): $\delta = 11.4$ (SiCH), 15.0 (CH₃), 18.8 (CH₃), 31.1 (CH₃), 31.2 (CH₃), 46.6 (SC), 47.0 (SC), 59.8 (OCH₂), 88.3 (C=C), 88.9 (C=C), 89.3 (C=C), 89.4 (C=C), 91.8 (C=C), 92.7 (C=C), 93.3(6) (C=C), 93.4 (C=C), 98.0 (C=C), 100.2 (C=C), 102.2, 104.6, 105.5, 119.8 (OCH), 123.3, 123.4, 123.4(5), 123.5, 123.7, 124.7, 125.3, 125.8, 128.6, 128.8, 130.1, 131.7, 131.8, 131.9(7) (2 C), 132.0, 133.3, 133.8, 134.7, 135.0, 137.0, 138.4, 138.9, 140.3, 140.9, 147.1 (OC), 147.6 (OC) ppm. C₆₀H₆₁O₃S₂Si (1049.24): calcd. C 68.68, H 5.86; found C 68.92, H 5.77. MS (FAB): m/z (%) = 1048.3 (1) [M]⁺, 961.2 (1) [M – C₄H₉ – 2 CH₃]⁺, 905.1 (1) [M – C₄H₉ – 2 C₃H₇]⁺, 849.1 (1) [M – C₄H₉ – 2 C₃H₇ – C₃H₆O + 2 H]⁺, 57.0 (100) [C₄H₉]⁺.

4-{[4-(tert-Butylsulfanyl)-2-((3-((5-(tert-butylsulfanyl)-2-iodophenyl)ethynyl)phenyl)ethynyl)phenyl]ethynyl}phenyl]ethynyl}-2-ethoxy-7-ethynyl-1,3-benzodioxole (13): TBAF (1 M solution in THF, 670 μL , 0.67 mmol) was added to a degassed solution of compound **12** (117 mg, 0.11 mmol) in THF (10 mL) containing one drop of glacial AcOH. The resulting solution was stirred at room temp. for 20 min and the solvents were evaporated. Flash chromatography (SiO₂, hexane/CH₂Cl₂, 70:30) afforded **13** (95 mg, 95%) as a white solid; m.p. 81–82 °C. $R_f = 0.30$ (SiO₂, hexane/CH₂Cl₂, 50:50). ¹H NMR (400 MHz, CDCl₃): $\delta = 1.23$ (t, $^3J_{\text{H,H}} = 7.2$ Hz, 3 H, CH₃), 1.31 [s, 9 H, C(CH₃)₃], 1.33 [s, 9 H, C(CH₃)₃], 3.36 (s, 1 H, =CH), 3.71 (q, $^3J_{\text{H,H}} = 7.1$ Hz, 2 H, OCH₂), 6.95 (d, $^3J_{\text{H,H}} = 8.4$ Hz, 1 H), 7.01 (s, 1 H, OCH), 7.02 (d, $^3J_{\text{H,H}} = 8.8$ Hz, 1 H), 7.16 (dd, $^3J_{\text{H,H}} = 8.0$, $^4J_{\text{H,H}} = 2.0$ Hz, 1 H), 7.36 (t, $^3J_{\text{H,H}} = 7.6$ Hz, 1 H), 7.38 (t, $^3J_{\text{H,H}} = 8.0$ Hz, 1 H), 7.48 (dd, $^3J_{\text{H,H}} = 7.8$, $^4J_{\text{H,H}} = 1.8$ Hz, 1 H), 7.50–7.60 (m, 5 H), 7.68 (d, $^4J_{\text{H,H}} = 2.4$ Hz, 1 H), 7.75 (d, $^4J_{\text{H,H}} = 1.2$ Hz, 1 H), 7.78 (t, $^4J_{\text{H,H}} = 1.6$ Hz, 1 H), 7.79 (t, $^4J_{\text{H,H}} = 1.6$ Hz, 1 H), 7.83 (d, $^3J_{\text{H,H}} = 8.0$ Hz, 1 H) ppm. ¹³C NMR (100 MHz, CDCl₃): $\delta = 14.8$ (CH₃), 31.1 (CH₃), 31.2 (CH₃), 46.6 (SC), 47.0 (SC), 59.7 (OCH₂), 77.4 (C=C), 83.3 (C=C), 88.3 (C=C), 88.5 (C=C), 89.2(8) (C=C), 89.3 (C=C), 91.8 (C=C), 92.7 (C=C), 93.5 (C=C), 93.6 (C=C), 102.2, 103.8, 105.2, 119.9 (OCH), 123.3, 123.4, 123.5, 123.6, 124.9, 125.3, 125.6, 125.8, 128.6, 128.8, 130.0, 131.7, 131.8, 131.8(5), 131.9, 132.0, 133.3, 134.0, 134.7, 135.0, 137.0, 138.4, 138.9, 140.3, 140.8, 147.0 (OC), 147.8 (OC) ppm. C₅₁H₄₁O₃S₂ (892.90): calcd. C 68.60, H 4.63; found C 68.85, H 4.79. MS (FAB): m/z (%) = 892.2 (4) [M]⁺, 791.2 (1) [M – C₄H₉ – C₂H₅O + H]⁺, 735.1 (1) [M – 2 C₄H₉ – C₂H₅O + 2 H]⁺, 706.1 (1) [M – 2 C₄H₉ – C₃H₆O₂ + 2 H]⁺, 609.2 (1) [M – 2 C₄H₉ – C₂H₅O – I + 3 H]⁺, 57.0 (100) [C₄H₉]⁺.

7,28-Bis(tert-butylsulfanyl)-37-ethoxy-36,38-dioxahexacyclo[32.5.2.1^{12,16}.1^{19,23}.0^{4,9}.0^{26,31}.0^{35,39}]tritetraconta-1(39),4,6,8,12(43),13,15,19(42),20,22,26,28,30,34,40-pentadecaene-2,10,17,24,32-pentayne (6): Pd(PPh₃)₄ (123 mg, 0.11 mmol) and CuI (21 mg, 0.11 mmol) were added to a degassed solution of compound **13** (95 mg, 0.11 mmol) in a mixture of toluene (500 mL) and *i*Pr₂NEt (1.5 mL). The resulting solution was stirred at room temp. overnight and the solvents were evaporated. Flash chromatography (SiO₂, hexane/CH₂Cl₂, 65:35) afforded **6** (34 mg, 42%) as a yellow solid; m.p. above 250 °C (decomposition). $R_f = 0.28$ (SiO₂, hexane/CH₂Cl₂, 50:50). ¹H NMR (400 MHz, CDCl₃): $\delta = 1.20$ (t, $^3J_{\text{H,H}} = 7.0$ Hz, 3 H, CH₃), 1.34 [s, 18 H, C(CH₃)₃], 3.71 (q, $^3J_{\text{H,H}} = 7.1$ Hz, 2 H, OCH₂), 7.18 (s, 2 H), 7.37 (t, $^3J_{\text{H,H}} = 7.6$ Hz, 2 H), 7.38 (s, 1

H, OCH), 7.48 (dd, $^3J_{\text{H,H}} = 8.0$, $^4J_{\text{H,H}} = 1.6$ Hz, 2 H), 7.52 (dt, $^3J_{\text{H,H}} = 7.9$, $^4J_{\text{H,H}} = 1.5$ Hz, 2 H), 7.54–7.57 (m, 4 H), 7.75 (d, $^4J_{\text{H,H}} = 1.6$ Hz, 2 H), 7.90 (t, $^4J_{\text{H,H}} = 1.4$ Hz, 2 H) ppm. ¹³C NMR (100 MHz, CDCl₃): $\delta = 14.7$ (CH₃), 31.2 (CH₃), 47.0 (SC), 60.2 (OCH₂), 88.5 (C=C), 88.6 (C=C), 89.5 (C=C), 93.5 (C=C), 93.7 (C=C), 105.2, 119.9 (OCH), 123.2, 123.7, 124.9, 125.8, 125.9, 128.7, 131.6, 131.8, 131.9, 133.9, 135.6, 137.0, 140.2, 147.3 (OC) ppm. C₅₁H₄₀O₃S₂·0.5H₂O (774.00): calcd. C 79.14, H 5.34; found C 79.24, H 5.47. MS (EI): m/z (%) = 764.2 (100) [M]⁺, 708.0 (11) [M – C₄H₉ + H]⁺, 652.2 (53) [M – 2 C₄H₉ + 2 H]⁺, 596.1 (5) [M – 2 C₄H₉ – C₃H₆O + 4 H]⁺, 57.1 (29) [C₄H₉]⁺.

S,S'-[35,36-Dihydroxyhexacyclo[32.2.2.1^{12,16}.1^{19,23}.0^{4,9}.0^{26,31}]tetraconta-1(36),4,6,8,12(40),13,15,19(39),20,22,26,28,30,34,37-pentadecaene-2,10,17,24,32-pentayne-7,28-diy] Diethanethioate (1): Boron tribromide (1 M in CH₂Cl₂, 650 μL , 0.65 mmol) was added in five equal portions over 4 h to a degassed solution of compound **6** (49 mg, 64.0 μmol) in a mixture of dry toluene (12 mL) and acetyl chloride (3 mL). The resulting solution was stirred at room temp. for 1 h. The solution was poured onto ice and the product was extracted with CH₂Cl₂. The combined organic layers were dried with MgSO₄, filtered and the solvents evaporated to dryness. Flash chromatography (SiO₂, CH₂Cl₂/MeOH, 100:0 to 99:1) afforded **1** (28 mg, 64%) as a brown solid; m.p. > 370 °C. $R_f = 0.26$ (SiO₂, CH₂Cl₂/MeOH, 99:1). ¹H NMR (400 MHz, CDCl₃): $\delta = 2.47$ (s, 6 H, CH₃), 6.43 (s, 2 H, OH), 7.10 (s, 2 H), 7.35 (t, $^3J_{\text{H,H}} = 7.6$ Hz, 2 H), 7.37 (dd, $^3J_{\text{H,H}} = 8.0$, $^4J_{\text{H,H}} = 1.6$ Hz, 2 H), 7.50 (dt, $^3J_{\text{H,H}} = 7.9$, $^4J_{\text{H,H}} = 1.3$ Hz, 2 H), 7.52 (dt, $^3J_{\text{H,H}} = 7.6$, $^4J_{\text{H,H}} = 1.4$ Hz, 2 H), 7.60 (d, $^3J_{\text{H,H}} = 8.0$ Hz, 2 H), 7.66 (d, $^4J_{\text{H,H}} = 1.6$ Hz, 2 H), 8.09 (t, $^4J_{\text{H,H}} = 1.4$ Hz, 2 H) ppm. ¹³C NMR (125 MHz, CDCl₃): $\delta = 30.5$ (CH₃), 88.2 (C=C), 89.4 (C=C), 89.5 (C=C), 94.3 (C=C), 95.7 (C=C), 111.0, 123.0, 123.2, 123.6, 125.8, 126.2, 128.6, 128.8, 131.4, 131.8, 132.4, 134.0, 136.3, 137.9, 145.0 (C-OH), 193.1 (C=O) ppm. C₄₄H₂₄O₄S₂·2.2H₂O (720.42): calcd. C 73.36, H 3.97; found C 73.43, H 4.03. MS (FAB): m/z (%) = 719.3 (1) [M + K]⁺, 681.2 (1) [M + H]⁺, 680.3 (1) [M]⁺, 38.9 (100).

Crystal Data for 6: C₅₁H₄₀O₃S₂, $M = 765.01$, $F(000) = 804$, yellow plate, size 0.03 × 0.13 × 0.27 mm³, triclinic, space group $P\bar{1}$, $Z = 2$, $a = 10.3054(5)$ Å, $b = 13.7858(8)$ Å, $c = 14.4700(8)$ Å, $\alpha = 97.504(3)^\circ$, $\beta = 98.777(3)^\circ$, $\gamma = 97.825(3)^\circ$, $V = 1988.54(19)$ Å³, $D_{\text{calcd.}} = 1.278$ Mg m⁻³. The crystal was measured on a KappaAPEX diffractometer at 123 K by using graphite-monochromated Mo- K_α radiation with $\lambda = 0.71073$ Å, $\theta_{\text{max}} = 30.033^\circ$. Minimal/maximal transmission 0.98/0.99, $\mu = 0.178$ mm⁻¹. The Apex2 program package^[51] has been used for data collection and integration. From a total of 85370 reflections, 11615 were independent (merging $r = 0.032$). From these, 8429 were considered as observed [$I > 2.0\sigma(I)$] and were used to refine 568 parameters. The structure was solved by direct methods using the program SIR92.^[52] Least-squares refinement against F was carried out on all non-hydrogen atoms using the program CRYSTALS.^[53] $R = 0.0448$ (observed data), $wR = 0.0739$ (all data), GOF = 1.1177. Minimal/maximal residual electron density $-0.32/0.46$ e Å⁻³. Chebyshev polynomial weights^[54] were used to complete the refinement. Plots were produced using Ortep3 for Windows.^[55]

CCDC-737782 contains the supplementary crystallographic data (excluding structure factors) for compound **6**. These data can be obtained free of charge from The Cambridge Crystallographic Data Centre via www.ccdc.cam.ac.uk/data_request/cif.

Electrochemistry: All electrochemical measurements were performed with an Autolab PGSTAT12 (Metrohm) and a conventional three-electrode system comprising a glassy carbon (GC)

working electrode (2 mm diameter rod), a platinum gauze as the auxiliary electrode and a Ag/AgCl/KCl_{3M} reference electrode. The GC and reference electrodes were purchased from Metrohm. All potentials are reported vs. the Ag/AgCl reference electrode at room temperature. The GC electrode was successively polished in a 1.0, 0.3 and 0.05 μm alumina slurry prepared from dry alumina powder and Milli-Q water on microcloth pads (CH Instruments, Inc.). The electrode was thoroughly rinsed with Milli-Q water and sonicated in Milli-Q water for 5 min after each polishing step. The bare GC electrode has an electrochemical roughness factor (ratio of the electrochemical area to the geometrical area) of 1.22.

Single-Molecule Conductance Measurements: A break junction approach in a STM configuration was used to measure single-molecule conductances.^[49] Current-distance measurements were carried out at room temperature using a modified Molecular Imaging PicoSPM. The STM tips were uncoated, electrochemically etched gold wires (99.999%, 0.25 mm diameter, etching solution: 1:1 mixture of aq. 30% HCl and ethanol). 25 μM solutions of compounds **1** and **14** were freshly prepared in a 4:1 mixture of mesitylene and THF. The acetyl protecting groups were cleaved in situ upon addition of 8 μM tetrabutylammonium hydroxide. The Au(111) electrodes used in this work were freshly flame-annealed gold discs of 2 mm height and 10 mm in diameter. A commercial STM scanner modified with a dual channel preamplifier^[56] and combined with a digital oscilloscope Yokogawa DL 750 were used to acquire the stretching data.

The following protocol was applied. Firstly, the STM tip was controlled at a preset tunnelling position (e.g. 100 pA). Then the feedback was switched off and the tip approached the substrate until the tunnelling current reached a preset value (e.g. 50 μA). After a duration of 100 ms sufficiently long to ensure the formation of stable metal nanocontact, the tip was retracted at a rate of about 60 nm s⁻¹ to a specified distance. Simultaneously, the transient conductance curves were recorded. The cycle was repeated up to 3000 times to obtain a sufficiently large database ensuring a reliable subsequent statistical analysis. The experiments were carried out in a glass chamber filled with high-purity argon to prevent oxygen exposure and contamination from air. The data for each molecule were recorded with three different bias voltages (0.065, 0.10 and 0.17 V).

Data Analysis and Conductance Histograms: Data saved in a binary format were analyzed with a lab-built software implemented into the graphical language LabView 8.6. The data analysis was similar to the method proposed by Venkataraman et al.^[57] In general, plateaus in between abrupt changes in conductance were collected to build the conductance histogram. Firstly, for each conductance trace Median Filter was applied to smooth the plateau region, but not the abrupt drops. Secondly, the negative derivative was computed and a Savitzky–Golay Filter was then applied to smooth this derivative. Thirdly, all peaks above a certain threshold were considered further. Fourth, the length between two successive peaks was calculated. Only plateaus longer than 0.05 nm were processed further. Fifth, mean value, standard deviation and slope (linear fit) of the plateau region were used for further selection. Finally, if a plateau is selected, the untreated data points of plateau region were used to build the conductance histogram. All these conductance histograms were summed up. When all data were processed, the peaks in the conductance histograms were fitted with log-normal distribution shown below.

$$f(x; \mu, \sigma) = y_0 + \frac{A}{x\sigma\sqrt{2\pi}} \exp\left(-\frac{(\ln(x) - \mu)^2}{2\sigma^2}\right)$$

Acknowledgments

The authors acknowledge the generous support of the Volkswagen Foundation (to N.W., T.W. and M.M.), the Gebert-Rüf Foundation (to Y.L. and M.M.), the Deutsche Forschungsgemeinschaft (to A.M. and T.W.) and the Schweizerischer Nationalfonds. We also thank A. Rudnev for complementary CV studies.

- [1] N. Weibel, S. Grunder, M. Mayor, *Org. Biomol. Chem.* **2007**, *5*, 2343–2353.
- [2] N. J. Tao, *Nat. Nanotechnol.* **2006**, *1*, 173–181.
- [3] C. Joachim, M. A. Ratner, *Proc. Natl. Acad. Sci. USA* **2005**, *102*, 8801–8808.
- [4] J. R. Heath, M. A. Ratner, *Phys. Today* **2003**, *56*, 43–49.
- [5] R. L. Carroll, C. B. Gorman, *Angew. Chem. Int. Ed.* **2002**, *41*, 4378–4400.
- [6] C. Joachim, J. K. Gimzewski, A. Aviram, *Nature* **2000**, *408*, 541–548.
- [7] L. Venkataraman, Y. S. Park, A. C. Whalley, C. Nuckolls, M. S. Hybertsen, M. L. Steigerwald, *Nano Lett.* **2007**, *7*, 502–506.
- [8] J. G. Kushmerick, A. S. Blum, D. P. Long, *Anal. Chim. Acta* **2006**, *568*, 20–27.
- [9] A. Salomon, D. Cahen, S. Lindsay, J. Tomfohr, V. B. Engelkes, C. D. Frisbie, *Adv. Mater.* **2003**, *15*, 1881–1890.
- [10] R. E. Holmlin, R. F. Ismagilov, R. Haag, V. Mujica, M. A. Ratner, M. A. Rampi, G. M. Whitesides, *Angew. Chem. Int. Ed.* **2001**, *40*, 2316–2320.
- [11] J. Reichert, R. Ochs, D. Beckmann, H. B. Weber, M. Mayor, H. von Löhneysen, *Phys. Rev. Lett.* **2002**, *88*, 176804/1–176804/4.
- [12] M. Mayor, H. B. Weber, J. Reichert, M. Elbing, C. von Hänisch, D. Beckmann, M. Fischer, *Angew. Chem. Int. Ed.* **2003**, *42*, 5834–5838.
- [13] M. Mayor, C. von Hänisch, H. B. Weber, J. Reichert, D. Beckmann, *Angew. Chem. Int. Ed.* **2002**, *41*, 1183–1186.
- [14] E. Lörtscher, M. Elbing, M. Tschudy, C. von Hänisch, H. B. Weber, M. Mayor, H. Riel, *ChemPhysChem* **2008**, *9*, 2252–2258.
- [15] S. Wu, M. T. González, R. Huber, S. Grunder, M. Mayor, C. Schönberger, M. Calame, *Nat. Nanotechnol.* **2008**, *3*, 569–574.
- [16] R. Huber, M. T. González, S. Wu, M. Langer, S. Grunder, V. Horhoiu, M. Mayor, M. R. Bryce, C. Wang, R. Jitchati, C. Schönberger, M. Calame, *J. Am. Chem. Soc.* **2008**, *130*, 1080–1084.
- [17] M. Elbing, R. Ochs, M. Koentopp, M. Fischer, C. von Hänisch, F. Weigend, F. Evers, H. B. Weber, M. Mayor, *Proc. Natl. Acad. Sci. USA* **2005**, *102*, 8815–8820.
- [18] S. Grunder, R. Huber, V. Horhoiu, M. T. González, C. Schönberger, M. Calame, M. Mayor, *J. Org. Chem.* **2007**, *72*, 8337–8344.
- [19] A. Błaszczuk, M. Chadim, C. von Hänisch, M. Mayor, *Eur. J. Org. Chem.* **2006**, 3809–3825.
- [20] D. Dulić, S. J. van der Molen, T. Kudernac, H. T. Jonkman, J. J. D. de Jong, T. N. Bowden, J. van Esch, B. L. Feringa, B. J. van Wees, *Phys. Rev. Lett.* **2003**, *91*, 207402/1–207402/4.
- [21] Z. Li, I. Pobelov, B. Han, T. Wandlowski, A. Błaszczuk, M. Mayor, *Nanotechnology* **2007**, *18*, 044018/1–044018/8.
- [22] Z. Li, B. Han, G. Meszaros, I. Pobelov, T. Wandlowski, A. Błaszczuk, M. Mayor, *J. Chem. Soc. Faraday Trans.* **2006**, *131*, 121–143.
- [23] I. V. Pobelov, Z. Li, T. Wandlowski, *J. Am. Chem. Soc.* **2008**, *130*, 16045–16054.
- [24] C. Li, A. Mishchenko, Z. Li, I. Pobelov, T. Wandlowski, X. Q. Li, F. Würthner, A. Bagrets, F. Evers, *J. Phys.: Condens. Matter* **2008**, *20*, 374122/1–374122/11.
- [25] E. Lörtscher, J. W. Ciszek, J. Tour, H. Riel, *Small* **2006**, *2*, 973–977.

- [26] A. S. Blum, J. G. Kushmerick, D. P. Long, C. H. Patterson, J. C. Yang, J. C. Henderson, Y. Yao, J. M. Tour, R. Shashidhar, B. R. Ratna, *Nat. Mater.* **2005**, *4*, 167–172.
- [27] Y. Luo, C. P. Collier, J. O. Jeppesen, K. A. Nielsen, E. DeIonno, G. Ho, J. Perkins, H.-R. Tseng, T. Yamamoto, J. F. Stoddart, J. R. Heath, *ChemPhysChem* **2002**, *3*, 519–525.
- [28] J. Chen, M. A. Reed, A. M. Rawlett, J. M. Tour, *Science* **1999**, *286*, 1550–1552.
- [29] E. H. van Dijk, D. J. T. Myles, M. H. van der Veen, J. C. Hummelen, *Org. Lett.* **2006**, *8*, 2333–2336.
- [30] J. K. Sørensen, M. Vestergaard, A. Kadziola, K. Kilså, M. B. Nielsen, *Org. Lett.* **2006**, *8*, 1173–1176.
- [31] F.-R. F. Fan, J. Yang, L. Cai, D. W. Price Jr., S. M. Dirk, D. V. Kosynkin, Y. Yao, A. M. Rawlett, J. M. Tour, A. J. Bard, *J. Am. Chem. Soc.* **2002**, *124*, 5550–5560.
- [32] S. Tsoi, I. Griva, S. A. Trammell, A. S. Blum, J. M. Schnur, N. Lebedev, *ACS Nano* **2008**, *2*, 1289–1295.
- [33] N. Weibel, A. Błaszczuk, C. von Hänisch, M. Mayor, I. Pobelov, T. Wandlowski, F. Chen, N. Tao, *Eur. J. Org. Chem.* **2008**, 136–149.
- [34] J. M. Seminario, A. G. Zacarias, J. M. Tour, *J. Am. Chem. Soc.* **2000**, *122*, 3015–3020.
- [35] J. Chen, M. A. Reed, *Chem. Phys.* **2002**, *281*, 127–145.
- [36] K. Stokbro, J. Taylor, M. Brandbyge, P. Ordejón, *Ann. N. Y. Acad. Sci.* **2003**, *1006*, 212–226.
- [37] J. Taylor, M. Brandbyge, K. Stokbro, *Phys. Review B* **2003**, *68*, 121101/1–121101/4.
- [38] W. Zhang, J. S. Moore, *Angew. Chem. Int. Ed.* **2006**, *45*, 4416–4439.
- [39] S. Höger, *Chem. Eur. J.* **2004**, *10*, 1320–1329.
- [40] Y. Yamaguchi, Z.-i. Yoshida, *Chem. Eur. J.* **2003**, *9*, 5430–5440.
- [41] D. Zhao, J. S. Moore, *Chem. Commun.* **2003**, 807–818.
- [42] T. C. Bedard, J. S. Moore, *J. Am. Chem. Soc.* **1995**, *117*, 10662–10671.
- [43] O. Hirata, M. Takeuchi, S. Shinkai, *Chem. Commun.* **2005**, 3805–3807.
- [44] Z. Zhu, T. M. Swager, *Org. Lett.* **2001**, *3*, 3471–3474.
- [45] H. Kukula, S. Veit, A. Godt, *Eur. J. Org. Chem.* **1999**, 277–286.
- [46] N. A. Bumagin, A. B. Ponomaryov, I. P. Beletskaya, *Synthesis* **1984**, 728–729.
- [47] S. Anderson, *Chem. Eur. J.* **2001**, *7*, 4706–4714.
- [48] N. Zhu, W. Hu, S. Han, Q. Wang, D. Zhao, *Org. Lett.* **2008**, *10*, 4283–4286.
- [49] C. Li, I. Pobelov, T. Wandlowski, A. Bagrets, A. Arnold, F. Evers, *J. Am. Chem. Soc.* **2008**, *130*, 318–326.
- [50] X. Xiao, L. A. Nagahara, A. M. Rawlett, N. Tao, *J. Am. Chem. Soc.* **2005**, *127*, 9235–9240.
- [51] Bruker AXS Inc., Madison, **2006**.
- [52] A. Altomare, G. Cascarano, C. Giacovazzo, A. Guagliardi, M. C. Burla, G. Polidori, M. Camalli, *J. Appl. Crystallogr.* **1994**, *27*, 435.
- [53] P. W. Betteridge, J. R. Carruthers, R. I. Cooper, K. Prout, D. J. Watkin, *J. Appl. Crystallogr.* **2003**, *36*, 1487.
- [54] J. R. Carruthers, D. J. Watkin, *Acta Crystallogr., Sect. A* **1979**, *35*, 698–699.
- [55] L. J. Farrugia, *J. Appl. Crystallogr.* **1997**, *30*, 565.
- [56] G. Mészáros, C. Li, I. Pobelov, T. Wandlowski, *Nanotechnology* **2007**, *18*, 424004/1–424004/8.
- [57] Y. S. Park, A. C. Whalley, M. Kamenetska, M. L. Steigerwald, M. S. Hybertsen, C. Nuckolls, L. Venkataraman, *J. Am. Chem. Soc.* **2007**, *129*, 15768–15769.

Received: July 7, 2009

Published Online: November 3, 2009